Elastic and inelastic scattering of 50 MeV pions from ^{12}C, ^{32}S, and ^{34}S

R. J. Sobie and T. E. Drake
Physics Department, University of Toronto, Toronto, Ontario, Canada M5S 1A7

K. L. Erdman, R. R. Johnson, H. W. Roser, and R. Tacik
Physics Department, University of British Columbia, Vancouver, British Columbia, Canada V6T 2A6

E. W. Blackmore and D. R. Gill
TRIUMF, Vancouver, British Columbia, Canada V6T 2A3

S. Martin
Institut für Kernphysik, Kernforschungsanlage Jülich, D-5170 Jülich, Federal Republic of Germany

C. A. Wiedner
Max-Planck-Institut für Kernphysik, D-6900 Heidelberg, Federal Republic of Germany

T. Masterson
Nuclear Physics Laboratory, University of Colorado, Boulder, Colorado 80309
(Received 13 July 1984)

Angular distributions for elastic and inelastic scattering of 50 MeV pions from ^{12}C, ^{32}S, and ^{34}S are reported. The elastic scattering data are fitted with an optical model in configuration space. Distorted wave calculations reproduce the inelastic $\pi^{\pm}$ data. The extracted neutron and proton matrix elements are consistent with measurements using other probes.

I. INTRODUCTION

A complete understanding of nuclear structure requires an understanding of both neutron and proton effects in the nucleus. While there are a number of techniques for isolating these effects in nuclei, none have the sensitivity that the low energy pion appears to have. Some low energy pion measurements of ground state neutron and proton densities have been recently reported in the literature,[1,2] but in this paper we focus on the ability of the low energy pion to separate neutron and proton matrix elements for transitions between the ground state and the low lying excited states of the nucleus.[3]

Pion inelastic scattering near the (3,3) resonance has been shown to be useful in determining neutron and proton transition matrix elements.[4] Here the elementary pion-nucleon interaction is dominated by the resonance in the $l=1$, $J=\frac{3}{2}$, $T=\frac{3}{2}$ partial wave and the π^+p to π^-p amplitude ratio is 3. However, at energies below the (3,3) resonance, the pion-nucleon interaction suggests a larger sensitivity to neutron and proton effects. At $T_\pi=50$ MeV the ratio of the π^+p to π^-p differential cross sections varies rapidly with angle, increasing from ~ 1 at $\theta=90°$ to greater than 20 at $\theta>120°$. Thus, at backward angles the π^- interacts only with the neutron and the π^+ only with the proton. In contrast to resonance energy pions, where the sensitivity to neutrons and protons can be explained in terms of the isospin coupling, this large difference between the π^+p and π^-p differential cross sections at $T_\pi=50$ MeV is due to constructive and destructive interference between the s and p wave parts of the pion-nucleon interaction.

We have measured the $\pi^{\pm}$ elastic and inelastic scattering cross sections for ^{12}C, ^{32}S, and ^{34}S. Before presenting the inelastic scattering results, we first compare calculations using pion-nucleus optical potentials, which are based on a global analysis of π^+ elastic scattering and pionic atom data, to the π^- elastic cross sections measured here. Then, to demonstrate the reliability of the low energy pion probe, we will show that the low energy pion scattering yields transition matrix elements for the first 2^+ states that are consistent with electron scattering measurements and with electromagnetic lifetime measurements for the $N=Z$ nuclei ^{12}C and ^{32}S. Finally, we determine the neutron and proton transition matrix elements for the first 2^+ state in ^{34}S and compare them to existing data.

II. EXPERIMENTAL DETAILS

The experiment was performed at the $M13$ pion channel using the quadrupole-quadrupole-dipole (QQD) pion spectrometer at TRIUMF. A detailed description of the channel and the spectrometer is presented elsewhere.[5,6] Briefly, the pion channel delivers an achromatic beam of low energy pions ($T_\pi \leq 50$ MeV) to the scattering target. The scattered pions are then momentum analyzed in the QQD spectrometer, which consists of two quadrupoles and a single dipole magnet, bending in the horizontal plane. The trajectory of the pion is measured by four multiwire proportional counters located in the spectrometer. The pion tracks are then fitted in order to determine

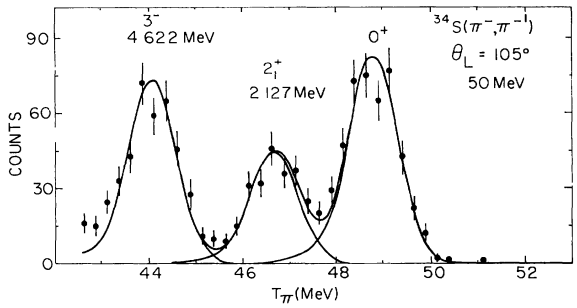

FIG. 1. Spectrum of 50 MeV π^- projectiles scattered from ^{34}S at 105°. The ground state and 2_1^+ state are clearly isolated.

the initial target position and momentum. The combined channel-spectrometer resolution for these measurements was typically 0.9—1.2 MeV for $T_\pi = 50$ MeV pions. A spectrum of negative pions scattered from ^{34}S at $\theta = 105°$ is shown in Fig. 1. The ground state and first 2^+ (2.13 MeV) state are clearly isolated. The large peak, tentatively identified as the 3^- (4.62 MeV) state, may have other states contributing.

Elastic scattering data were taken for CH_2, ^{32}S, and ^{34}S targets for laboratory angles from 40 to 130 deg and the inelastic scattering data were taken from 60 to 130 deg (see Table I). The 50 MeV pion fluxes on the scattering targets were 2×10^6 π^+/s and 4×10^5 π^-/s for a momentum spread of the pion beam in the channel of $\Delta p/p = 0.5\%$. The pion flux was measured by a pair of in-beam scintillation counters and a muon decay monitor.[7] The measured muon and electron contamination in the incident beam was typically 7% and 9% for π^+ and π^-, respectively, and this was easily removed by time-of-flight measurements using the cyclotron rf signal.[6]

The absolute solid angle of the spectrometer was determined by measuring the yield of pions scattered from the hydrogen in a CH_2 target at various angles and normalizing to the π^+p differential cross section of the phase shift calculation of Arndt *et al.*,[8] which is based on fits to the low energy scattering data of Bertin *et al.*[9] The solid angle was 14—16 msr, depending on the size of the beamspot on the scattering target. The overall normalization error is ±10% for the ^{12}C data and ±15% for the sulfur data, due to solid angle and target thickness uncertainties.

III. EXPERIMENTAL RESULTS

Configuration space calculations were done with a distorted wave code DWPI (Ref. 10) modified to handle the Michigan State University (MSU) pion-nucleus potential.[11] Further modifications were made in order to separately take into account the neutron and proton ground state and inelastic transition densities. The elastic and inelastic cross sections were analyzed with the MSU pion-nucleus optical potential,[12—14] which has the form

$$\frac{2\omega}{4\pi}U_{\rm opt} = -b(r) + B_0\rho^2 + \vec{\nabla}\cdot\left[\frac{L(r)}{1+4\pi\lambda/3\cdot L(r)}\right]\vec{\nabla} + \tfrac{1}{2}\nabla^2[c(r)+C_0\rho^2] ,$$

where

$$b(r) = \bar{b}_0\rho - \epsilon_\pi b_1\delta\rho ,$$

$$L(r) = c(r) + C_0\rho^2 ,$$

$$c(r) = c_0\rho - \epsilon_\pi c_1\delta\rho ,$$

with ϵ_π being the pion charge, A the atomic weight, and ω the total pion energy. The kinematic factors have been omitted for simplicity.

This form of the pion-nucleus potential was chosen, rather than the usual Kisslinger form,[15] since the various terms in the potential can be related to specific processes. The imaginary parts of the b_0, b_1, c_0, and c_1 terms describe attenuation processes (inelastic scattering, quasi-elastic scattering, etc.), while the $\mathrm{Im}B_0$ and $\mathrm{Im}C_0$ terms describe pionic atom and pion absorption data. There are nine isoscalar and four isovector terms to determine in the MSU potential. Due to a lack of data on $N\neq Z$ nuclei, the isovector terms b_1 and c_1 are fixed at their phase shift values. The omission of isovector terms for pion absorption is supported by pionic atom data and by low energy pion absorption data.[14] The imaginary parts of b_0 and c_0 were taken from a pion-nucleon phase shift analysis, but reduced by the Pauli factor $Q=0.31$. Since these terms are relatively small, a ±50% variation in their value produces little effect in the scattering cross section. The imaginary parts of B_0 and C_0 were determined at zero pion kinetic energy by pionic atom data. The energy variation of the s-wave B_0 and p-wave C_0 absorption terms was assumed to be the same from 0 to 50 MeV, thus the ratio $\mathrm{Im}B_0/\mathrm{Im}C_0$ is kept constant at the pionic atom value when $\mathrm{Im}B_0$ and $\mathrm{Im}C_0$ are varied to fit the cross sections. It has been pointed out by the MSU group[14] and by Seki and Masutani,[16] that the real parts of the terms b_0 and B_0 (as well as c_0 and C_0) are not independent of each other. The MSU group fixed the $\mathrm{Re}B_0$ and $\mathrm{Re}C_0$ to theoretical values and varied the $\mathrm{Re}b_0$, $\mathrm{Re}c_0$, and the absorption terms to fit a wide body of π^+ elastic scattering cross sections. An in-depth discussion of the MSU optical potential can be found in Refs. 12—14.

The parameter set "set-E" for the MSU potential is able to describe π^+ 30, 40, and 50 MeV cross sections of closed-shell nuclei from ^{12}C to ^{208}Pb. A single set of parameters for each energy could reasonably describe the π^+ data for all of these nuclei, and only small energy variations were needed. This contrasts to intermediate energy proton scattering, where the optical model parameters vary more rapidly with A and with energy.[17] In adjusting the pion-nucleus potential to fit the data measured here, we follow the MSU prescription by only varying the $\mathrm{Re}b_0$ and $\mathrm{Re}c_0$, as well as the absorption terms $\mathrm{Im}B_0$ and $\mathrm{Im}C_0$, but keeping the absorption ratio fixed at the pionic atom values. The remaining parameters are fixed at the set-E values.

A. Elastic scattering

The π^+ ^{12}C elastic differential cross section at 50 MeV has been measured by several groups.[18—20] Good agreement is obtained with the π^+ data of Moinester *et al.*,[18] which has the smallest uncertainty. The data of Dytman

TABLE I. Table of cross sections (center-of-mass) (errors shown are due to statistics).

θ (deg)	$\frac{d\sigma}{d\Omega}(\pi^+)$ (mb/sr)	$\frac{d\sigma}{d\Omega}(\pi^-)$ (mb/sr)	$\frac{d\sigma}{d\Omega}(\pi^+)$ (mb/sr)	$\frac{d\sigma}{d\Omega}(\pi^-)$ (mb/sr)
	^{12}C elastic		^{12}C(2$^+$,4.44 MeV)	
39.3	7.36±0.30	20.8 ±1.5		
49.4	4.43±0.18	8.56±0.61		
59.5	2.75±0.07	3.12±0.19	0.117±0.014	0.184±0.028
70.9	2.65±0.06		0.154±0.012	
72.2		2.27±0.13		0.166±0.033
81.0	4.04±0.08	3.73±0.20	0.230±0.014	0.265±0.030
90.4		5.59±0.25		0.58 ±0.08
92.3	5.24±0.12		0.398±0.020	
102.3	6.27±0.19	6.77±0.25	0.592±0.045	0.98 ±0.08
111.6	6.47±0.18			
112.2		6.64±0.27	0.94 ±0.07	1.33 ±0.10
122.1	6.47±0.23	6.40±0.28	1.40 ±0.07	1.75 ±0.11
131.5	5.55±0.26	5.75±0.30	1.52 ±0.10	2.22 ±0.15
	^{32}S elastic		^{32}S(2$^+$,2.23 MeV)	
38.9	31.7 ±1.8	66.1 ±5.7		
49.0	15.3 ±0.9	29.7 ±2.7		
59.0	11.2 ±0.5	13.4 ±0.9		
70.3	11.2 ±0.6			
80.3	10.6 ±0.6	12.6 ±1.0	0.53 ±0.10	0.64 ±0.07
90.3		10.1 ±0.5		0.90 ±0.07
91.6	9.7 ±0.5		0.79 ±0.10	
101.6	7.32±0.38	4.75±0.35	1.08 ±0.12	0.99 ±0.12
105.3		3.10±0.21		1.05 ±0.09
111.0	4.90±0.30		1.11 ±0.08	
111.6		1.78±0.15		1.19 ±0.13
121.6	3.90±0.34	0.58±0.09	1.18 ±0.12	1.19 ±0.12
131.1	2.94±0.19	0.86±0.11	1.27 ±0.11	0.91 ±0.11
	^{34}S elastic		^{34}S(2$^+$,2.13 MeV)	
38.9	31.6 ±2.0	81.9 ±7.4		
49.0	15.8 ±1.0	28.8 ±2.2		
59.0	10.4 ±0.6	13.7 ±1.2		
70.3	8.7 ±0.3			
71.6		13.5 ±1.5		
80.3	9.7 ±0.4	13.1 ±0.7	0.51±0.07	0.45±0.06
90.3		10.4 ±0.6		0.96±0.09
91.6	8.54±0.51		0.63±0.07	
101.6	6.65±0.43	4.08±0.32	0.82±0.07	1.08±0.07
105.3		2.36±0.21		1.36±0.12
110.0	4.31±0.24		0.83±0.07	
111.6		1.02±0.16		1.16±0.14
121.6	3.06±0.23	0.31±0.13	0.98±0.08	1.21±0.14
131.1	2.44±0.19	1.27±0.14	0.96±0.08	1.07±0.10

et al.[19] and Johnson *et al.*[20] have large error bars, but are consistent with the results measured here. No 50 MeV π^- data have been published.

The results of fits to the ^{12}C elastic cross sections are presented in Table II and shown in Fig. 2. For ^{12}C, we have used a Gaussian point-nucleon density distribution ($c=1.57$ fm and $a=1.33$ fm) determined from electron scattering. The solid curve in Fig. 2 is a calculation using the MSU parameter set-E for the optical potential. We observe that it does rather poorly at backward angles for both π^+ ($\chi^2=35$) and π^- ($\chi^2=22$). The MSU group found in their analysis that the best fit to the π^+ elastic cross sections of closed-shell nuclei from ^{12}C to ^{208}Pb was obtained when the ImB_0 and ImC_0 absorption terms were 60% of the pionic atom values. If we allow the Reb_0 and Rec_0 terms to vary, we can find a reasonable simultaneous fit (potential 1 in Table II) to the π^+ and π^- ^{12}C elastic cross section data (dashed curve in Fig. 2). In addition, if we allow the absorption terms ImB_0 and ImC_0 to vary, but fix the ratio ImB_0/ImC_0 at the pionic atom

TABLE II. Optical model parameters.[a]

Nucleus	Data fitted	Potential number	$\mathrm{Re}b_0$ (fm)	$\mathrm{Re}c_0$ (fm^3)	$\frac{\mathrm{Im}B_0{}^{b}}{\mathrm{Im}C_0}$	χ^2
	Phase shift values		−0.042	0.73		
^{12}C	$\pi^{\pm}$	1	−0.053±0.004	0.65±0.03	60%	5.0
	$\pi^{\pm}$	2	−0.054±0.004	0.64±0.03	80%	2.8
	π^{+}	3	−0.053±0.004	0.67±0.03	60%	7.1
	π^{+}	4	−0.053±0.004	0.66±0.03	80%	2.1
	π^{-}	5	−0.054±0.004	0.63±0.03	60%	1.1
	π^{-}	6	−0.055±0.004	0.64±0.03	80%	2.5
^{32}S	$\pi^{\pm}$	7	−0.067±0.005	0.52±0.03	60%	4.3
	π^{+}	8	−0.052±0.005	0.67±0.03	60%	3.1
	π^{-}	9	−0.060±0.006	0.50±0.03	60%	2.6
^{34}S[c]	π^{+}	8	−0.052	0.67	60%	3.0
	π^{-}	9	−0.060	0.50	60%	3.9

[a]Unspecified parameters are fixed at MSU set-E values.
[b]Units are a percentage of the pionic atom values ($\mathrm{Im}B_0=-0.19$ fm^4, $\mathrm{Im}C_0=0.93$ fm^6).
[c]No parameters were varied for π^+ ^{34}S. The neutron ground state density parameters were varied for π^- ^{34}S.

value, we find a minimum near 80% of the pionic atom values with the same $\mathrm{Re}b_0$ and $\mathrm{Re}c_0$ parameters (see potential 2 in Table II). The values of these parameters determined when the π^+ and π^- ^{12}C elastic cross sections are separately fitted are unchanged from the simultaneous fit (see potentials 3–6 in Table II).

For ^{32}S, a two-parameter Fermi density was used to describe the neutron and proton ground state distributions. The parameters were taken from an analysis of elastic electron scattering form factors.[21] For the proton distributions, c_p was adjusted to reproduce the rms radius of the point-proton distribution ($c_p=3.13$ fm and $t_p=2.41$ fm). The neutron density of ^{32}S was assumed to be identical to the proton density. We find that the π^+ elastic scattering data of ^{32}S is fairly well described by the MSU set-E potential ($\chi^2=9$), while the fit to the π^- elastic scattering data is poor ($\chi^2=82$) (solid line in Fig. 3). This trend has also been noted in other low energy π^- elastic scattering data[22] and is perhaps expected, since the MSU potential is based on a large set of π^+ elastic scattering data between 20 and 50 MeV, but very little π^- elastic data.

To fit the π^+ and π^- ^{32}S elastic data, we varied $\mathrm{Re}b_0$ and $\mathrm{Re}c_0$ and the absorption terms ($\mathrm{Im}B_0$ and $\mathrm{Im}C_0$) in the optical potential. The best fit to the ^{32}S data is obtained when the absorption terms are 80% of the pionic atom values; however, the fit is only slightly better than that for 60%. Thus, the results we present have the absorption terms fixed at 60% of the pionic atom values (same as MSU set-E). In Table II, we present the results of varying the $\mathrm{Re}b_0$ and $\mathrm{Re}c_0$ terms to fit the $\pi^{\pm}$ data, first simultaneously (see potential 7) and then separately (see potentials 8 and 9). In contrast to the ^{12}C results where the potentials determined from separate fits to the π^+ and π^- data were identical, the potentials determined from separate fits to the π^+ ^{32}S and π^- ^{32}S data are different. The potential that describes the π^+ ^{32}S data (potential 8) has a significantly stronger p-wave ($\mathrm{Re}c_0$) strength than the potential that describes the π^- ^{32}S data (potential 9). However, the potential that simultaneously fits both the π^+ and π^- ^{32}S data (potential 7) is very similar to the potential that fits the π^- ^{32}S data (potential 9), but not the π^+ ^{32}S data. This may reflect the fact that the π^- cross section spans two orders of magnitude, while the π^+ only one, thus suggests that the π^- elastic cross sections may be more sensitive to the optical potential parameters than the π^+.

For the analysis of the ^{34}S elastic cross sections we used a two-parameter Fermi distribution for the point proton density. The parameters determined from elastic electron scattering are $c_p=3.20$ fm and $t_p=2.39$ fm.[21] Since variations of the neutron density c_n and t_n parameters do not change the π^+ elastic cross section, and similarly, small variations of c_p and t_p do not change the π^- elastic cross section, we varied the neutron density c_n and t_n to fit the π^- data. No parameters were varied in the π^+ ^{34}S calculations and we find the π^+ ^{32}S potential (potential 8) gives a good fit to the π^+ ^{34}S elastic data. Fits to the π^- ^{34}S elastic data using the π^- ^{32}S potential (potential 9) give neutron density parameters $c_n=3.28\pm0.10$ fm and $t_n=2.38\pm0.10$ fm. The results are presented in Table II and shown in Fig. 4. A complete discussion of the sensitivity of low energy pions to ground state neutron and proton density distributions in magnesium and sulfur isotopes is given in Ref. 23 and it will not be pursued here.

B. Inelastic scattering results

1. Collective model calculations

In order to calculate the inelastic cross sections, we have chosen to parametrize the transition density from the ground state to the first 2^+ states with the Tassie model density.[24] This model for the transition density has been

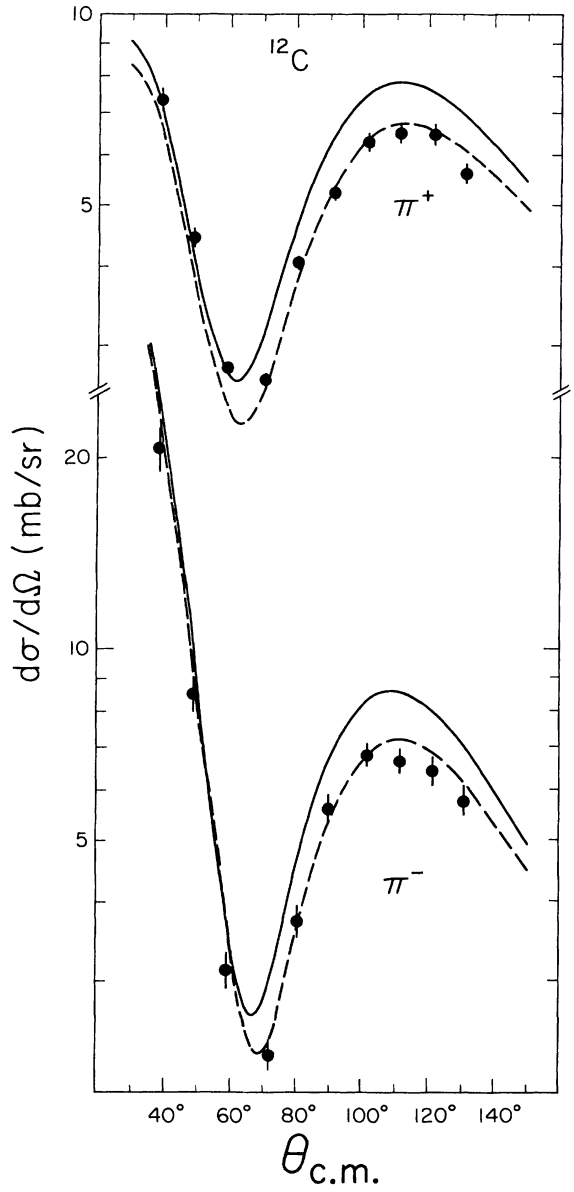

FIG. 2. Angular distribution for elastic scattering of 50 MeV $\pi^{\pm}$ on ^{12}C. The solid curves are the result of optical model calculations using the parameters of MSU set-E and the dashed curves are the best fit to the data when the absorption parameters are 60% of the pionic atom values.

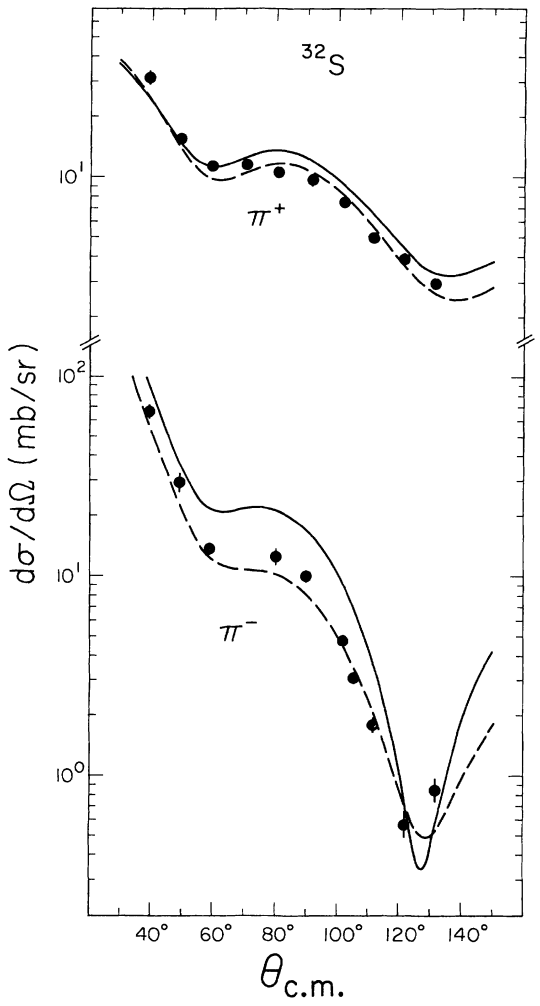

FIG. 3. Angular distribution for elastic scattering of 50 MeV $\pi^{\pm}$ on ^{32}S. The solid curves are the result of optical model calculations using the parameters of MSU set-E and the dashed curves are the best fit (potentials 8 and 9 in Table II) to the data.

used in both intermediate energy proton scattering (for example, see Ref. 25) and in pion scattering (for example, see Ref. 26). But more important, $B(E\lambda)$ values are extracted from the electron scattering data with the Tassie model.[27]

The Tassie model density has the form

$$\rho_{tr}(\vec{r})=\beta Y_{20}(\Omega_r)r\frac{d\rho_c}{dr}$$

for a $0^+\rightarrow 2^+$ transition. The deformation parameter β determines the strength of the transition, and the density ρ_c is typically a two-parameter Fermi density. Since the interaction is uncertain, inelastic hadron scattering cannot accurately measure the strength and radial dependence of the transition density simultaneously. This is especially true of pions at forward angles in the region of the s-p wave interference minimum. However, at backward angles in the 2^+ diffraction maximum, one can determine the strength of the transition. The radial dependence of the transition density can be determined from electron scattering form factors with parameters (c, t, and β) by fitting the relation

$$F(q)=\left[B(E2,0^+\rightarrow 2^+)\frac{4\pi}{Z^2}\right]^{1/2}\int_0^\infty \rho_{tr}(r)j_2(qr)r^2dr\ ,$$

where F is the longitudinal electromagnetic form factor and $\rho_{tr}(r)$ is the radial part of the Tassie model density. For the 2^+ (4.44 MeV) state in ^{12}C, the data of Sick and McCarthy[28] were used, while for ^{32}S and ^{34}S, the longitudinal electron scattering form factors of the first 2^+ states from Ref. 29 were used.

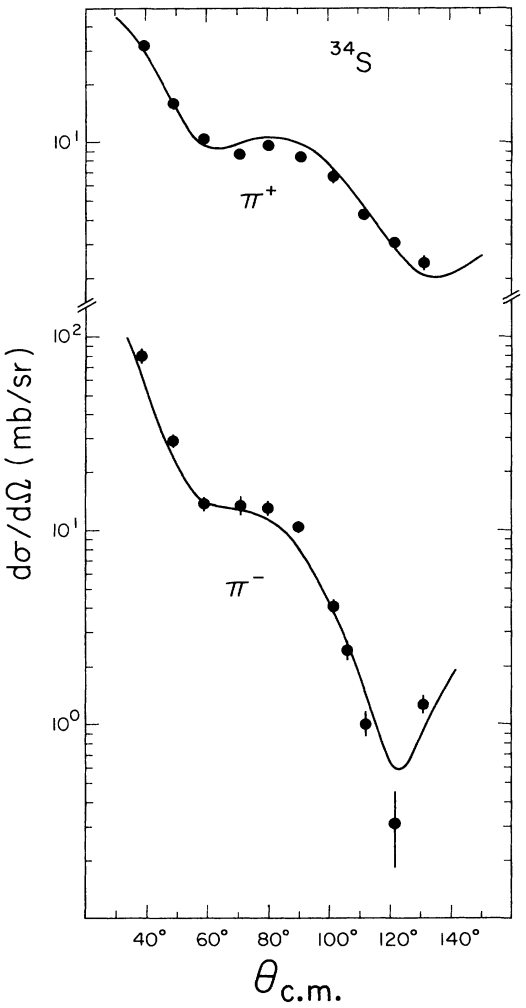

FIG. 4. Angular distribution for elastic scattering of 50 MeV $\pi^{\pm}$ on ^{34}S. The curves are the result of optical model calculations using the parameters of the best-fit potential (potentials 8 and 9 in Table II) of ^{32}S. The proton density parameters were taken from electron scattering measurements, while the neutron ground state density parameters were varied to fit the data.

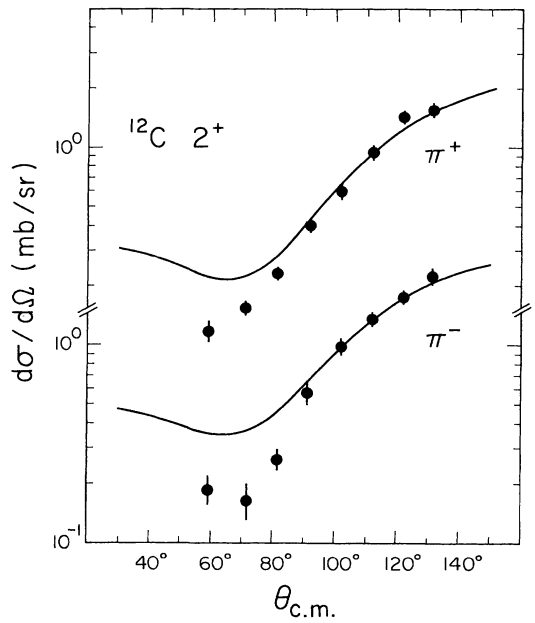

FIG. 5. Angular distribution for inelastic scattering of 50 MeV $\pi^{\pm}$ to the 4.44 2$^+$ state in ^{12}C. The curves are the result of DWPI calculations. The deformation parameters deduced are $\beta_{\pi+}=0.59$ and $\beta_{\pi-}=0.55$ when the absorption parameters are 80% of the pionic atom value.

In the $N=Z$ nuclei, ^{12}C and ^{32}S, the neutron and proton transition densities are assumed to be identical. Thus, the neutron deformation parameter β_n and proton deformation parameter β_p are equal, and the transition density can be parametrized by a single deformation parameter β_π. For the ^{12}C and ^{32}S 2$^+$ cross sections, we varied the deformation parameter to fit the π^+ cross sections to get $\beta_{\pi+}$ and we varied the deformation parameter to fit the π^- cross sections to get $\beta_{\pi-}$. A good check of the consistency of the pion-nucleus potential is obtained as $\beta_{\pi+}=\beta_{\pi-}$ from charge symmetry.

Neutron M_n and M_p reduced transition matrix ele-

TABLE III. Summary of inelastic scattering results for ^{12}C and ^{32}S.

Nucleus	Data fitted	Potential number	Reb_0 (fm)	Rec_0 (fm^3)	$\frac{\text{Im}B_0{}^a}{\text{Im}C_0}$	β	χ^2	$\frac{\beta_{\pi+}}{\beta_{\pi-}}$
^{12}C	π^+	1	−0.053	0.67	60%	0.55±0.05	1.7	1.08±0.08
	π^-	1	−0.053	0.67	60%	0.51±0.05	0.2	
^{12}C	π^+	2	−0.053	0.66	80%	0.59±0.05	2.6	1.07±0.08
	π^-	2	−0.053	0.66	80%	0.55±0.05	0.3	
^{32}S	π^+	7	−0.067	0.52	60%	0.355±0.039	0.6	1.12±0.07
	π^-	7	−0.067	0.52	60%	0.316±0.035	1.4	
^{32}S	π^+	8	−0.052	0.67	60%	0.325±0.036	1.2	0.95±0.06
	π^-	9	−0.060	0.50	60%	0.343±0.038	1.5	

[a]Units are percentage of pionic atom values.

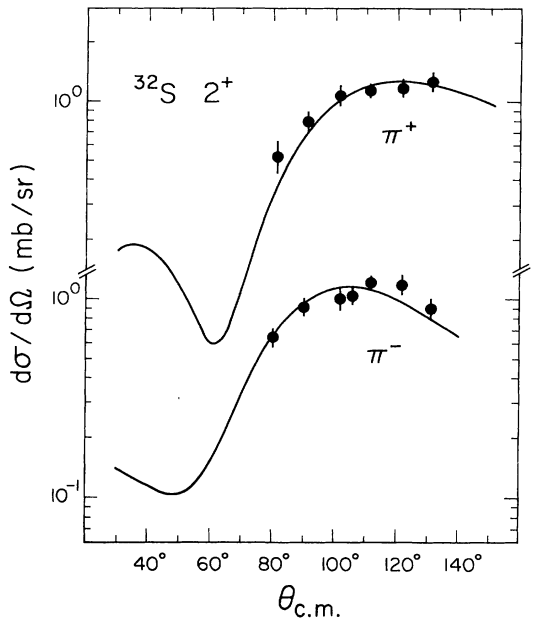

FIG. 6. Angular distributions for inelastic scattering of 50 MeV $\pi^{\pm}$ to the 2.23 MeV 2$^+$ state in ^{32}S. The curves are the result of DWPI calculations. The deformation parameters deduced are $\beta_{\pi^+}=0.325$ and $\beta_{\pi^-}=0.343$.

ments can be calculated from

$$M_n = Ne \int r^2 Y^*_{20}(\Omega_r)\rho^n_{tr}(\vec{r})d\vec{r}$$

and

$$M_p = Ze \int r^2 Y^*_{20}(\Omega_r)\rho^p_{tr}(\vec{r})d\vec{r},$$

where $\rho^n_{tr}(\vec{r})$ and $\rho^p_{tr}(\vec{r})$ are the respective neutron and proton transition densities. For ^{34}S, we have assumed that the neutron transition density has the same radial shape as the proton transition density and they differ only in the deformation parameter. Thus the matrix element ratio M_p/M_n is equal to $Z\beta_p/N\beta_n$.

Since the Tassie model fit to the electron scattering form factor gives a deformation parameter, as well as the radial parameters of the transition density, we can compare this to the measured pion deformation parameter. We can also compare the pion results to lifetime measurements, since in the long-wavelength limit

$$B(E2;0^+\rightarrow 2^+) = |M_p|^2 = \left[Ze\frac{5}{4\pi}\beta\langle r^2_{tr}\rangle\right]^2.$$

Cross sections for the 2$^+$ (4.44 MeV) state in ^{12}C have been previously measured with 50 MeV π^+ projectiles.[19] We find reasonable agreement between their data and the results obtained here. In Table III and Fig. 5, we show the results of calculations for the 2$^+$ (4.44 MeV) state in ^{12}C, where β_{π^+} and β_{π^-} deformation parameters were varied separately. The error on the deformation parameters includes the overall normalization error, while the ratio of the deformation parameters only includes the relative normalization error. The value of the deformation parameter is determined primarily by the backward angle data, away from the s-p interference minimum. Therefore only data points with $\theta \geq 90°$ were included. Inclusion of the data points with $\theta < 90°$ results in poor fits to the data. From electron scattering, $\beta=0.62\pm0.06$, and from lifetime measurements, $\beta=0.59\pm0.30$,[30] so it appears that the deformation parameters ($\beta=\beta_{\pi^+}=\beta_{\pi^-}$) obtained from the pion data are in good agreement with electron scattering and lifetime measurements.

The results of the fits of the first 2$^+$ (2.23 MeV) state in ^{32}S are presented in Table III and shown in Fig. 6. The cross sections were fitted by varying the deformation parameters β_{π^+} for the π^+ data and β_{π^-} for the π^- data separately. Our first observation is that the deformation parameters are essentially the same whether the absorption terms in the potentials are 60% or 80% of the pionic atom values, and hence, only the former are shown. However, if we use one potential that describes both the π^+ and π^- ^{32}S elastic data simultaneously (see potential 7 in Table II), the deformation parameters will differ from those where we use two potentials that separately describe the π^+ and π^- ^{32}S data (potentials 8 and 9 in Table II). In this section, we suggest that a consistency check of the pion-nucleus potential would be $\beta_{\pi^+}=\beta_{\pi^-}$. When the different π^+ and π^- potentials are used, the result is consistent with unity, $\beta_{\pi^+}/\beta_{\pi^-}=0.95\pm0.06$. But when the same potential for π^+ and π^- is used, the result is $\beta_{\pi^+}/\beta_{\pi^-}--=1.12\pm0.07$. The absolute error on the deformation parameters includes the $\pm15\%$ normalization error on the ^{32}S cross sections, while the ratio $\beta_{\pi^+}/\beta_{\pi^-}$ only includes the relative errors. The absolute value of the deformation parameters are consistent with the deformation parameters determined from lifetime measurements $\beta=0.286\pm0.016$,[13] and electron scattering $\beta=0.28\pm0.05$.

For ^{34}S, we have simultaneously fitted the π^+ and π^- cross sections of the first 2$^+$ (2.13 MeV) state by varying the proton β_p and the neutron β_n deformation parameters. When the different π^+ and π^- potentials are used (potentials 8 and 9 in Table III, which gives $\beta_{\pi^+}/\beta_{\pi^-}\sim1$ in ^{32}S), we find $\beta_p=0.283\pm0.032$, $\beta_n=0.287\pm0.032$, and $\beta_p/\beta_n=0.99\pm0.07$ with $\chi^2=3.7$ (see Fig. 7). Whereas, when the identical π^+ and π^- potentials are used (potential 7 in Table III, which gives $\beta_{\pi^+}/\beta_{\pi^-}\sim1.12$ for ^{32}S), we find $\beta_p=0.304\pm0.033$, $\beta_n=0.270\pm0.030$, and $\beta_p/\beta_n=1.13\pm0.09$ with $\chi^2=2.8$. The errors on β_p and β_n include the normalization error, while the ratio β_p/β_n only includes the relative error. Also, the ratio β_p/β_n is found to be insensitive to $\pm30\%$ variations in the isovector optical potential parameters Reb_1 and Rec_1. The absolute value of the proton deformation parameter is consistent with the deformation parameters determined from electron scattering $\beta_p=0.23\pm0.03$ and from lifetime measurements $\beta_p=0.24\pm0.01$.

We can relate the ratio of the deformation parameters to the matrix elements by recalling that $M_p/M_n=Z\beta_p/N\beta_n$, which for the 2$^+$ state of ^{34}S gives $M_p/M_n=0.88\pm0.06$ ($\beta_p/\beta_n=0.99\pm0.07$). The transition matrix elements M_p and M_n for $E2$ transitions are simply related to the isoscalar and isovector matrix elements M_0 and M_1 by $M_{p/n}=M_0\pm M_1T_z$ and thus, in an isospin triplet, $M_n(T_z)=M_p(-T_z)$. For $A=34$, there are

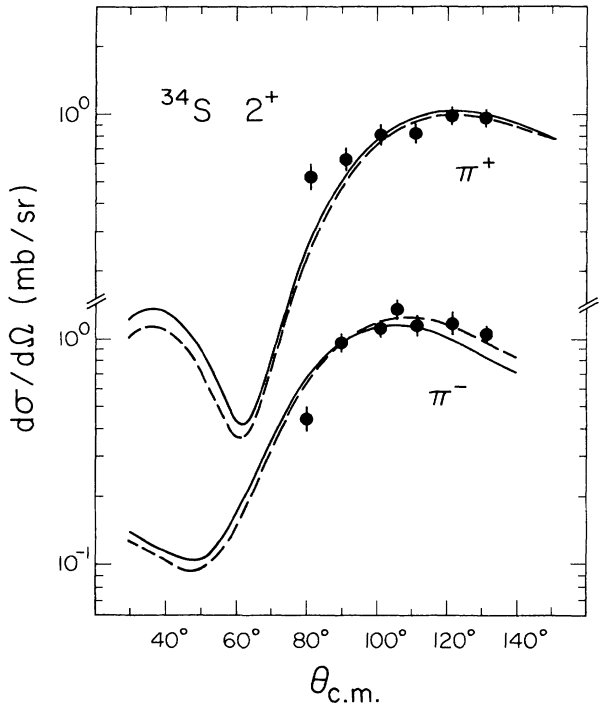

FIG. 7. Angular distributions for inelastic scattering of 50 MeV $\pi^{\pm}$ to the 2.13 MeV 2^+ state in ^{34}S. The solid curves are the result of collective model DWPI calculations. The neutron and proton deformation parameters were varied separately to fit the data, giving $\beta_p=0.283$ and $\beta_n=0.287$. The dashed curves use microscopic transition densities and the calculation has been normalized upward by approximately 20% to fit the data.

lifetime measurements for the first 2^+ $T=1$ states in ^{34}S, ^{34}Cl, and ^{34}Ar.[31] If we fit the three M_p values to the relation $M_p=M_0+M_1T_z$ and calculate M_n, we find that $M_p/M_n=0.72\pm0.10$. Although our results indicate a larger ratio than the lifetime measurements, we have not corrected the mirror nuclei M_p/M_n value for the Coulomb interaction. Presently there is some uncertainty in the value of this correction. For example, Alexander *et al.*[32] multiplied their M_p/M_n value, determined by measuring the lifetimes of the $E2$ transitions in the $A=26$ isospin triplet, by a factor of 1.1. For the Coulomb correction to $A=34$ nuclei, a similar correction would make the mirror nuclei value agree with the pion value.

A recent paper investigating *sd*-shell nuclei with 650 and 800 MeV protons has done an analysis of ^{34}S very similar to that done here.[25] They used a Tassie model density (with ground state parameters) and assumed that $M_p/M_n=0.72$. The results of a distorted-wave impulse approximation (DWIA) calculation was approximately 20% too high. However, our experiment has indicated that M_n is $\sim$20% smaller than that used in their analysis. This might reduce the result of the DWIA calculation so that it would in fact agree with their data.

2. *Microscopic model calculations*

In addition to the collective model analysis, we have generated microscopic transition densities for the first 2^+ states in ^{32}S and ^{34}S using shell model wave functions of Brown *et al.*[33] In this model, the ^{16}O core is assumed to be inert and the valence nucleons are allowed to occupy the $1d_{5/2}$, $2s_{1/2}$, and $1d_{3/2}$ orbitals. Instead of assuming a specific form for the residual interaction, the one- and two-body matrix elements are used as parameters to be varied in fits to a large body of energy level data. The wave functions are obtained by diagonalizing the resulting Hamiltonian matrix.

In the collective model analysis, we assumed that the neutron and proton transition densities had the same radial dependence and only differed by a deformation parameter. In ^{32}S, this is expected from charge symmetry ($N=Z$), however, in ^{34}S there are two extra neutrons and differences could occur. Therefore, we use the shell model to determine if the predicted radial dependence of the neutron transition density in ^{34}S is different from the proton density.

For the first 2^+ state in ^{32}S, the shell model predicts that $M_p=M_n$, and that the radial dependence of the neutron and proton transition densities is the same. With these shell model densities, the calculated π^+ and π^- cross sections (using potentials 8 and 9 in Table II) required an upward normalization of approximately 20% in the shell model calculation to fit the data. This result is consistent with that obtained in Sec. III B 1, and is expected, since the electron scattering form factors are in fact well described by this unnormalized shell model density.

For the first 2^+ state in ^{34}S, the shell model calculation predicts $M_p/M_n=0.92$ with slightly different neutron and proton transition densities. Using these shell model densities, the calculated π^+ and π^- cross sections also required an upward normalization of approximately 20% to fit the data (see Fig. 7). Thus, the shell model prediction of $M_p/M_n=0.92$ does fit the data and is consistent with our collective model analysis where $M_p/M_n=0.88\pm0.06$. It appears that our assumption, that the neutron and proton transition densities have the same radial shape, is valid for this state in ^{34}S. However, one must be careful, since the shell model calculation for other states such as the second 2^+ (3.30 MeV) state in ^{34}S predicts very different neutron and proton transition densities.

IV. SUMMARY

Elastic and inelastic scattering of π^+ and π^- projectiles by ^{12}C, ^{32}S, and ^{34}S have been studied at 50 MeV. The angular distributions for the elastic scattering have been compared with optical model calculations using the MSU pion-nucleus potential.[12–14] This form of the pion-nucleus potential, with parameter set-E, gives a reasonable description of the π^+ and π^- ^{12}C, as well as the π^+ ^{32}S and ^{34}S elastic cross sections. Improved fits to the data are obtained when the s-wave and p-wave strength terms and the absorption terms are slightly adjusted.

In contrast, the π^- ^{32}S and ^{34}S cross sections are poorly fitted with the MSU set-E potential, and to fit the π^- cross sections the p-wave strength had to be reduced by approximately 30%. It has been shown that a potential which describes both the π^+ and π^- ^{32}S cross sections can be obtained, but it failed to describe the $\pi^{\pm}$ ^{12}C and

other 50 MeV π^+ cross sections. Furthermore, we have pointed out that agreement with the inelastic scattering data is slightly better when the different π^+ and π^- potentials are used in the sulfur analysis. Elastic scattering of 65 MeV $\pi^\pm$ from ^{40}Ca by Dam *et al.*[22] have also found that different π^+ and π^- potentials were needed, although Sternheim[34] claims that a single potential can describe both the π^+ and π^- data.

Intuitively we would have expected that the π^+ and π^- optical potentials would be identical. A closer examination reveals that small differences between the π^+ and π^- potentials may not be so unexpected due to the incomplete treatment of the Coulomb interaction. For example, the Coulomb-nuclear interference term $V_C V_n + V_n V_C$ and the nuclear term V_n^2 are arbitrarily dropped in the elastic calculation,[35] although for 65 MeV $\pi^\pm$ ^{40}Ca scattering Dam *et al.* has pointed out that the effect of these terms is small.[22] Also, the effect of the Coulomb interaction is not calculated exactly (i.e., nonrelativistically instead of relativistically).[35] Seki *et al.* have suggested that the minimum in the π^+ ^{208}Pb elastic cross section at 50 MeV is much deeper in a nonrelativistic treatment than in a relativistic one.[36] Even in recent charge symmetry $\pi^\pm$d experiments at resonance energy, a $\pi^\pm$ asymmetry appears that can only be explained when a complete calculation of Coulomb effects is done.[37] Furthermore, Ericson and Tauscher[38] have suggested that differences between the π^+ and π^- elastic scattering data in an $N=Z$ nucleus may be due to some energy dependence of the optical potential, since the Coulomb potential causes the π^- interaction to occur at higher pion kinetic energies than the π^+ interaction.

The inelastic cross sections were analyzed using transition densities obtained from electron scattering. Thus, direct comparisons of the pion results could be made to lifetime measurements, electron scattering, and proton scattering. For the $N=Z$ nuclei, ^{12}C and ^{32}S, the deformation parameters needed to describe the π^+ data should be equal to the deformation parameter needed to describe the π^- data from charge symmetry. For ^{12}C, the ratio of the deformation parameters was consistent with unity, and the absolute value of the deformation parameter (transition matrix element) is consistent with lifetime measurements and electron scattering. For ^{32}S, the ratio is 1.12 ± 0.07 when identical π^+ and π^- potentials are used and 0.95 ± 0.06 when different π^+ and π^- potentials are used. The absolute normalization is consistent with lifetime measurements and electron scattering.

For the inelastic cross sections of ^{34}S, the proton and neutron deformation parameters were varied to simultaneously fit both the π^+ and π^- cross sections. In the collective model analysis for the 2^+ state, we assumed that the neutron and proton transition densities have the same radial shape, but differ in the deformation parameter. We have confirmed this with a shell model calculation. The measured proton deformation parameter was found to be consistent in magnitude with lifetime measurements and electron scattering. The matrix element ratio $M_p/M_n = 0.88\pm0.06$ was found to be consistent with the M_p/M_n value obtained from mirror nuclei[31] and also with intermediate energy proton scattering.[25]

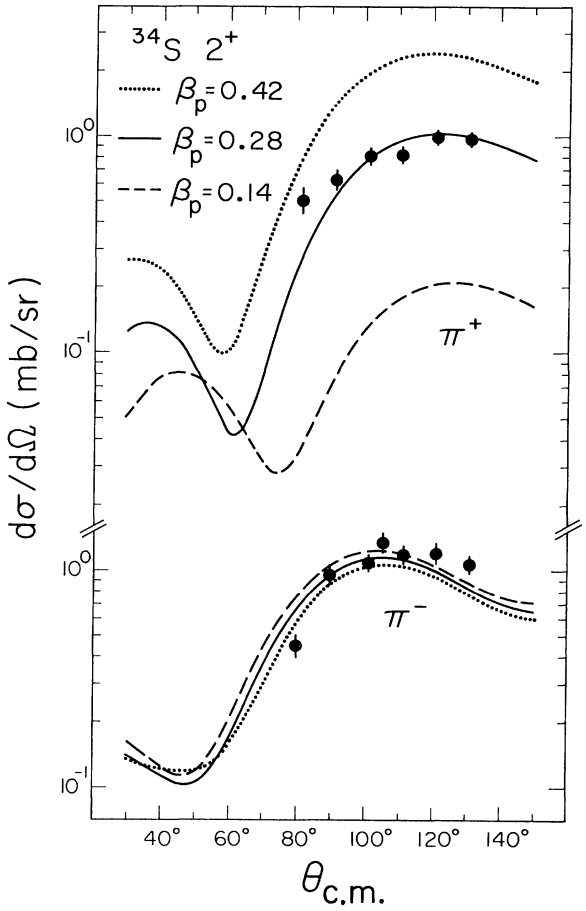

FIG. 8. Angular distributions for inelastic scattering of 50 MeV $\pi^\pm$ to the 2.13 MeV 2^+ state in ^{34}S. The solid curves are the best fit to the cross sections as shown in Fig. 7. The dotted curves have β_p increased 50% and the dashed curves have β_p decreased 50% over the best-fit value.

If low energy π^+ are sensitive only to protons and π^- are sensitive only to neutrons, as indicated by the π^+p and π^-p differential cross sections at 50 MeV, then a variation of β_p (β_n) should show a large change in the π^+ (π^-) inelastic cross section. in Fig. 8, we plot the 2^+ ^{34}S cross section with β_p increased and decreased 50% from the optimum value. For π^+ we see the cross section is very sensitive to β_p. However, changing β_p for π^- hardly affects the π^- cross section. Similar results are obtained for variations of β_n, thus suggesting that the 50 MeV pion is possibly the most sensitive probe for extracting the neutron and proton transition matrix elements.

In summary, we have shown that the 50 MeV pion can give results that are surprisingly consistent with other probes. Furthermore, the demonstrated consistency and the apparent sensitivity to neutron and proton transition matrix elements make the low energy pion an attractive probe for studying nuclear structure.

Support for this work was provided by the Natural Sciences and Engineering Research Council of Canada.

[1]R. R. Johnson, T. Masterson, B. Bassalleck, W. Gyles, T. Marks, K. L. Erdman, A. W. Thomas, D. R. Gill, E. Rost, J. J. Kraushaar, J. Alster, C. Sabev, J. Arvieux, and M. Krell, Phys. Rev. Lett. **43**, 844 (1979).

[2]B. M. Barnett, W. Gyles, R. R. Johnson, K. L. Erdman, J. Johnstone, J. J. Kraushaar, S. Lepp, T. G. Masterson, E. Rost, D. R. Gill, A. W. Thomas, J. Alster, I. Navon, and R. H. Landau, Phys. Lett. **97B**, 45 (1980).

[3]R. Tacik, K. L. Erdman, R. R. Johnson, H. W. Roser, D. R. Gill, E. W. Blackmore, R. J. Sobie, T. E. Drake, S. Martin, and C. A. Wiedner, Phys. Rev. Lett. **52**, 1276 (1984).

[4]S. Iverson, H. Namm, A. Obst, K. K. Seth, N. Tanaka, C. L. Morris, H. A. Thiessen, K. Boyer, W. Cottingame, C. F. Moore, R. L. Boudrie, and D. Dehnhard, Phys. Lett. **82B**, 51 (1979).

[5]C. J. Oram, J. B. Warren, G. M. Marshall, and J. Doornbos, Nucl. Instrum. Methods **179**, 95 (1981).

[6]R. J. Sobie, T. E. Drake, B. M. Barnett, K. L. Erdman, W. Gyles, R. R. Johnson, H. W. Roser, R. Tacik, E. W. Blackmore, D. R. Gill, S. Martin, C. A. Wiedner, and T. Masterson, Nucl. Instrum. Methods **219**, 501 (1984).

[7]E. A. Wadlinger, Nucl. Instrum. Methods **134**, 243 (1976).

[8]R. A. Arndt and L. D. Roper, Centre for Analysis of Particle Scattering, Internal Report CAPS-80-3, 1982.

[9]P. Y. Bertin, B. Coupat, H. Hivernat, B. B. Isabelle, J. Duclos, A. Gerard, J. Miller, J. Morgenstern, J. Picard, and R. Powers, Nucl. Phys. **B106**, 341 (1976).

[10]R. A. Einstein and R. A. Miller, Comput. Phys. Commun. **11**, 95 (1976).

[11]J. A. Carr (private communication).

[12]J. A. Carr, H. McManus, and K. Stricker-Bauer, Phys. Rev. C **25**, 952 (1982).

[13]K. Stricker, J. A. Carr, and H. McManus, Phys. Rev. C **22**, 2043 (1980).

[14]K. Stricker, H. McManus, and J. A. Carr, Phys. Rev. C **19**, 929 (1979).

[15]L. S. Kisslinger, Phys. Rev. **98**, 761 (1955).

[16]R. Seki and K. Masutani, Phys. Rev. C **27**, 2799 (1983).

[17]P. Schwandt, H. O. Meyer, W. W. Jacobs, A. D. Bacher, S. E. Vigdor, M. D. Kaitchuck, and T. R. Donoghue, Phys. Rev. C **26**, 55 (1982).

[18]M. A. Moinester, R. L. Burman, R. P. Redwine, M. A. Yates-Williams, D. J. Malbrough, C. W. Darden, R. D. Edge, T. Marks, S. H. Dam, B. M. Preedom, F. E. Bertrand, T. P. Cleary, E. E. Gross, C. A. Ludermann, M. Blecher, K. Gotow, D. Jenkins, and F. Milder, Phys. Rev. C **18**, 2678 (1978).

[19]S. A. Dytman, J. F. Amann, P. D. Barnes, J. N. Craig, K. G. R. Doss, R. A. Eisenstein, J. D. Sherman, W. R. Wharton, G. R. Burleson, S. L. Verbeck, R. J. Peterson, and H. A. Thiessen, Phys. Rev. C **19**, 971 (1979).

[20]R. R. Johnson, T. G. Masterson, K. L. Erdman, A. W. Thomas, and R. H. Landau, Nucl. Phys. **A296**, 444 (1978).

[21]D. Rychel, Ph.D. thesis, University of Mainz, 1983.

[22]S. H. Dam, R. D. Edge, B. M. Preedom, M. Hamm, R. L. Burman, R. Carlini, R. P. Redwine, M. A. Yates, M. Blecher, K. Gotow, F. E. Bertrand, E. E. Gross, and M. A. Moinester, Phys. Rev. C **25**, 2574 (1982).

[23]W. Gyles, Ph.D. thesis, University of British Columbia, 1984.

[24]L. J. Tassie, Aust. J. Phys. **9**, 407 (1956).

[25]R. A. Miskimen, A. M. Bernstein, B. Quinn, S. A. Wood, M. V. Hynes, G. S. Blampied, B. G. Ritchie, and V. R. Brown, Phys. Lett. **131B**, 26 (1983).

[26]C. L. Morris, K. G. Boyer, C. F. Moore, C. J. Harvey, K. J. Kallianpur, I. B. Moore, P. A. Seidl, S. J. Seestrom-Morris, D. B. Holtkamp, S. J. Greene, and W. B. Cottingame, Phys. Rev. C **24**, 231 (1981).

[27]R. P. Singhal, H. S. Caplan, J. R. Moreira, and T. E. Drake, Can. J. Phys. **51**, 2125 (1973).

[28]I. Sick and J. S. McCarthy, Nucl. Phys. **A150**, 631 (1970).

[29]D. Rychel (private communication).

[30]F. Ajenberg-Selove, Nucl. Phys. **A248**, 1 (1975).

[31]P. M. Endt and C. Van der Leun, Nucl. Phys. **A310**, 1 (1978).

[32]T. K. Alexander, G. C. Ball, W. G. Davies, J. S. Forster, I. V. Mitchell, and H. B. Mak, Phys. Lett. **113B**, 132 (1982).

[33]B. A. Brown, R. Radhi, and B. H. Wildenthal, Phys. Rep. **101**, 314 (1983).

[34]M. M. Sternheim, Phys. Rev. C **29**, 1140 (1984).

[35]R. A. Eisenstein and R. A. Miller, Comput. Phys. Commun. **8**, 130 (1974).

[36]R. Seki, K. Masutani, and K. Yazaki, Phys. Rev. C **27**, 2817 (1983).

[37]T. G. Masterson, J. J. Krausharr, R. J. Peterson, R. S. Raymond, R. A. Ristinen, R. L. Boudrie, E. F. Gibson, and A. W. Thomas, Phys. Rev. C **26**, 2091 (1982).

[38]T. E. O. Ericson and L. Tauscher, Phys. Lett. **112B**, 425 (1982).